

Article

Construction of a Nanosensor for Non-Invasive Imaging of Hydrogen Peroxide Levels in Living Cells

Amreen ¹, Hayssam M. Ali ², Mohammad Ahmad ^{3,*}, Mohamed Z. M. Salem ⁴  and Altaf Ahmad ¹ 

¹ Department of Botany, Faculty of Life Sciences, Aligarh Muslim University, Aligarh 202002, India; gauramreen95@gmail.com (A.); aahmad.bo@amu.ac.in (A.A.)

² Botany and Microbiology Department, College of Science, King Saud University, P.O. Box. 2455, Riyadh 11451, Saudi Arabia; hayhassan@ksu.edu.sa

³ Department of Physics, Syracuse University, New York, NY 13244, USA

⁴ Forestry and Wood Technology Department, Faculty of Agriculture (El-Shatby), Alexandria University, Alexandria 21545, Egypt; zidan_forest@yahoo.com

* Correspondence: moahmad@syr.edu

Received: 14 October 2020; Accepted: 25 November 2020; Published: 29 November 2020



Simple Summary: Spatially and temporally defined H₂O₂ signatures are essential parts of various signaling pathways. Therefore, monitoring H₂O₂ dynamics with high spatio-temporal resolution is significantly important to understand how this ubiquitous signaling molecule can control diverse cellular responses. In this study, we designed and characterized a Fluorescence Resonance Energy Transfer (FRET)-based genetically encoded H₂O₂ sensor that provides a powerful tool to monitor the spatio-temporal dynamics of H₂O₂ fluxes. We have used this sensor to monitor the flux of H₂O₂ in live cells under stress conditions. Using this sensor, real-time information of the H₂O₂ level can be obtained non-invasively and would help to understand the adverse effect of H₂O₂ on cell physiology and its role in redox signaling.

Abstract: Hydrogen peroxide (H₂O₂) serves fundamental regulatory functions in metabolism beyond the role as damage signal. During stress conditions, the level of H₂O₂ increases in the cells and causes oxidative stress, which interferes with normal cell growth in plants and animals. The H₂O₂ also acts as a central signaling molecule and regulates numerous pathways in living cells. To better understand the generation of H₂O₂ in environmental responses and its role in cellular signaling, there is a need to study the flux of H₂O₂ at high spatio-temporal resolution in a real-time fashion. Herein, we developed a genetically encoded Fluorescence Resonance Energy Transfer (FRET)-based nanosensor (FLIP-H₂O₂) by sandwiching the regulatory domain (RD) of OxyR between two fluorescent moieties, namely ECFP and mVenus. This nanosensor was pH stable, highly selective to H₂O₂, and showed insensitivity to other oxidants like superoxide anions, nitric oxide, and peroxynitrite. The FLIP-H₂O₂ demonstrated a broad dynamic range and having a binding affinity (K_d) of 247 μM. Expression of sensor protein in living bacterial, yeast, and mammalian cells showed the localization of the sensor in the cytosol. The flux of H₂O₂ was measured in these live cells using the FLIP-H₂O₂ under stress conditions or by externally providing the ligand. Time-dependent FRET-ratio changes were recorded, which correspond to the presence of H₂O₂. Using this sensor, real-time information of the H₂O₂ level can be obtained non-invasively. Thus, this nanosensor would help to understand the adverse effect of H₂O₂ on cell physiology and its role in redox signaling.

Keywords: H₂O₂; nanosensor; oxidative stress; fluxomics

1. Introduction

Reactive oxygen species (ROS) are short-lived and highly reactive molecules formed upon incomplete reduction in oxygen [1,2]. They are the key regulators of various biological processes like signaling and development in living organisms. The higher production of ROS was observed under biotic and abiotic stress conditions [3]. The ROS can lead to oxidation of lipids, proteins, and DNA, which causes oxidative stress and finally cell death [4,5]. Recently, H_2O_2 has been observed as a specific component of numerous signaling pathways as well as a well-known toxic molecule among all the ROS present inside the cells [6]. Initially, the detection of ROS in cells, tissues, and organs were performed using colorimetric methods exploiting compounds such as nitroblue tetrazolium and diaminobenzidine, but these methods did not allow real-time measurements of ROS in the cells [7,8]. Later on, detection of ROS was achieved by using various fluorescent probes such as 20,70-dichlorofluorescein diacetate, dihydroethidium (DHE), dihydro-20,4,5,6,7,70-hexafluoro fluorescein but these probes are difficult to deliver into living cells and cause the toxicity [9]. Various H_2O_2 -selective probes have been developed, which utilize a boronate-deprotection mechanism, and the detection approach depends on the selective H_2O_2 -mediated conversion of aryl boronates to phenols [10,11]. Attachment of various fluorescent molecules with aryl boronates produces a fluorescent product when it reacts with H_2O_2 . For investigating the changes in the endogenous level of H_2O_2 , monoboronate-based probes have been developed Peroxyfluor-1 (PF-1), Peroxyfluor-2 (PF-2), Peroxyfluor-3 (PF-3), Peroxy Orange 1 (PO1), and Peroxy Yellow 1 (PY1). Although the H_2O_2 localization studies have been improved through boronate-deprotection based probes, quantitative analysis of H_2O_2 generation is still challenging by using these probes. Specifically, the concentration of the probe can affect the signal from the single-wavelength emitting probes. To deal with this issue, a monoboronate-based Ratio Peroxyfluor 1 (RPF)-1 probe was developed, which detects H_2O_2 in a ratiometric manner and can potentially permit normalization to probe concentration. However, one disadvantage with this probe is that it cannot select one kind of ROS [12].

In recent years, single fluorescent protein probes have been developed, which allowed reversible *in vivo* detection of reactive oxygen species in cells [9,13]. These probes include roGFP [14] and HyPer [15], which are mainly based on oxidation-reduction processes between the H_2O_2 and the reduced probe and show fluorescence upon oxidation. There are several disadvantages of single fluorescent protein (FP) probes, as these probes are more sensitive to some factors, i.e., pH and probe photobleaching. Therefore, to quantify the definite concentration of an analyte is not very reliable [16]. Therefore, there is a requisite to develop a simple, reliable, and non-invasive ratiometric method for the determination of H_2O_2 in living cells. Genetically encoded fluorescent proteins (FPs) and sensitized emission Fluorescence Resonance Energy Transfer (FRET) (seFRET)-based sensors provide an alternate way to study the metabolite dynamics in living cells. seFRET measurements are simple, and having a high Spatio-temporal resolution, enable the tracking of fast molecular events (ms). Sensing of fast changes in metabolite dynamics and protein conformational changes is possible using the sensors based on FPs [17]. These kinds of sensors have been developed for non-invasive and specific detection of metal ions, amino acids, sugars, plant hormones [18–21].

In the present work, we developed a reliable tool, FLIP- H_2O_2 that can measure the concentration of H_2O_2 in a ratiometric manner and unlike the previously reported sensors, as their measurements are affected by auto-fluorescence [14], sensor protein concentrations, and excitation wavelength in lower visible region [16]. Some of them suffer from issues, such as cell toxicity [11,12], not being ideal for long term live cell imaging and pH sensitivity [16] FP and sensing domain-based sensors have several benefits in sensitivity and specificity over sensors made from traditional materials. They operate at a similar scale to natural biological process. All these factors make FLIP- H_2O_2 an attractive choice for visualizing H_2O_2 fluxes in living cells with an extended dynamic range. The regulatory domain (RD) of *E. coli* OxyR, a transcription factor, was exploited for sensing H_2O_2 along with green fluorescent protein (GFP) variants for the development of a H_2O_2 nanosensor. In order to develop this nanosensor, cyan emitting (ECFP, donor) and yellow emitting (mVenus, acceptor) particles were genetically fused

with the regulatory domain of an OxyR protein. The presence of H₂O₂ brought the conformational changes. This nanosensor utilizes the conformational change, and transfer of energy from the donor to acceptor fluorophore for monitoring of the H₂O₂. Flux of H₂O₂ was measured in the presence of different stress conditions in the living cells. Thus, this sensor can directly be expressed in a specific subset of cell populations and targeted to specific subcellular structures for in vivo detection and quantification of H₂O₂.

2. Materials and Methods

2.1. Chemicals, Vectors and Strains

All chemicals were purchased from Sigma-Aldrich (USA) unless otherwise specified. pDONR, pYES-DEST52 and pcDNA3.1(-) vectors were purchased from Thermo Fischer Scientific (USA). pGWF1 was purchased from Addgene (Watertown, MA, USA). *E. coli* strain DH5 alpha and BL21(DE3) from New England Biolabs (Beverly, MA, USA) were used for cloning and expression purpose. *Saccharomyces cerevisiae* (strain BY4742), kindly gifted by Yeast Resource Center (YRC), Washington, USA and HeLa cells purchased from ATCC (USA) were used for live cell imaging. Restriction enzymes were procured from New England Biolabs and Life technologies (USA). BP and LR clonase and other ligase enzymes were purchased from Thermo Fischer Scientific (USA). Nickel NTA (nitrilotriacetic acid) affinity chromatography columns, Imidazole, Ni²⁺- His bind resin were obtained from Novagen (USA).

2.2. Plasmid Construction

The regulatory domain (RD) of OxyR, a transcription factor of *Escherichia coli*, was found to sense H₂O₂. Therefore, it was used as the recognition element for developing the H₂O₂ nanosensor. The crystal structure of the protein was retrieved from RCSB-PDB (Research Collaboratory for Structural Bioinformatics-Protein Data Bank) (PDB ID-1I69, Supplementary Figure S1). The DNA sequence of the RD was extracted from the Kyoto Encyclopedia of Genes and Genomes (KEGG). ECFP and mVenus sequences were taken from addgene. ECFP and mVenus share a significant spectral overlap and Forster radius, which make this pair a good FRET pair. The nucleotide sequences of RD were amplified using *E. coli* K12 genomic DNA and gateway primers. 5'-GGG GAC AAG TTT GTA CAA AAA AGC AGG CTT CGA GAT GGC AAG CCA GCA GGG-3' that introduces attB1 site at the 5' end of the RD gene was used as forward primer. 5'-GGG GAC CAC TTT GTA CAA GAA AGC TGG GTC AAC CGC CTG TTT TAA AAC TTT-3' that introduces the attB2 site was used as the reverse primer. The amplified RD nucleotide sequence was cloned in the pDONR222 vector by using gateway cloning approach (BP clonase) and the entry clone was generated (Supplementary Figure S2). We selected pGWF1, a gateway destination plasmid, as a bacterial expression vector (addgene). The property of this vector is that it already contains ECFP and mVenus fluorescent tags and gateway attachment sites. The entry clone generated during BP reaction was further used for sub-cloning in the pGWF1 vector, and results in the development of the pGWF1_ECFP_RD_mVenus construct (Supplementary Figure S3) along with in-frame 6xHis tag). The construct was checked by restriction digestion and expected bands observed on agarose gel (Supplementary Figure S4). Nucleotide sequence fidelity was confirmed by Sanger sequencing (Supplementary Figure S5). The developed FRET nanosensor for H₂O₂ detection was named as FLIP-H₂O₂. The whole construct (ECFP-RD-mVenus) was further sub-cloned in pYES-DEST52 (Supplementary Figure S6) and pcDNA3.1 (Supplementary Figure S7) for expression in *Saccharomyces cerevisiae* and in mammalian cells, respectively.

2.3. Protein Expression and Purification

For the expression of recombinant construct, pGWF1_ECFP_RD_Venus construct was transformed to *E.coli*. The transformed cells were grown in Luria Bertini (LB) medium (HiMedia, India) containing

antibiotic (ampicillin 100 µg/mL) at 37 °C up to the OD₆₀₀ 0.6. The expression of sensor protein in bacterial cells was induced by using 1mM IPTG (Isopropyl β-D-1-thiogalactopyranoside) (HiMedia, India) and grown at 21 °C for 48 h under dark conditions due to the sensitivity of fluorophores for visible light. To harvest the expressed bacterial cells, the culture was centrifuged for 10 min at 4500 rpm. Then, supernatant was discarded. Resuspension of the pellet was done in 20 mM Tris-Cl buffer (pH 8.0) with 2-mercaptoethanol (5 mM, to keep the thiol group of the RD domain in reduced form), followed by bacterial cell lysis through ultrasonication and then centrifuged at 7000 rpm for 20 min to remove the cell debris. For the purification of nanosensor protein, supernatant was syringe filtered for the removal of remaining impurities and then loaded in a Ni-NTA resin packed column and incubated at 4 °C for 4 h for the efficient binding of the recombinant His-tagged protein with resin. Washing of the column was done with buffer containing Tris-Cl (20 mM) and imidazole (20 mM). Elution buffer (Tris-Cl-20 mM; imidazole-200 mM) was used to elute the sensor protein. The purified nanosensor protein was incubated overnight at 4 °C for proper folding to its native conformation. The purity and molecular weight of nanosensor protein was checked by SDS-PAGE analysis (Supplementary Figure S8).

2.4. In Vitro Characterization and Ligand Binding Affinity of Nanosensor Protein

The emission spectrum of the nanosensor was monitored by using an excitation filter 430 nm/20 nm for ECFP and taking emission intensities of the nanosensor in the range of 400 to 600 nm using the spectrofluorometer (LS50B Perkin Elmer, USA). For other measurements of ECFP and mVenus emission intensities, 480 nm/20 nm and 530 nm/25 nm filters of microplate reader (Synergy H1, Biotek, USA) were used, respectively. Certain in vitro tests were also performed to check the stability and specificity of nanosensor protein in different buffer systems PBS (Phosphate buffer saline), MOPS (3-(N-morpholino) propanesulfonic acid), Tris-Cl, and TBS (Tris-buffered saline). Furthermore, the stability of nanosensor protein was also checked in pH from 5.0–8.0 in the presence of H₂O₂ (1 µM) and the absence of H₂O₂. The PBS buffer at pH 7.0 was found to be suitable and selected for further analysis. The FRET ratio was recorded after adding the 20 µL of ligand with 180 µL of the diluted protein sample. The ligand titration curve was obtained by titrating purified protein with different concentration of H₂O₂, ranging from nanomolar to millimolar. The affinity of nanosensor protein (K_d) was determined by using the change in mVenus/ECFP ratio (FRET ratio) after binding with H₂O₂ by applying the ligand titration curves to the equation: $S = (r - r_{apo}) / (r_{sat} - r_{apo}) = [H_2O_2] / (K_d + [H_2O_2])$, where S is saturation; r is ratio; r_{apo} is ratio in the absence of H₂O₂; r_{sat} is ratio at saturation with H₂O₂.

2.5. In Vivo Characterization in Bacterial Cells

The pGWF1_ECFP_RD_Venus transformed bacterial cells (*E. coli* BL21) were grown in LB medium at 37 °C for in vivo analysis of the nanosensor. Expression of the nanosensor protein was induced by adding 1 mM IPTG (Isopropyl β-D-1-thiogalactopyranoside) to the cultured bacterial cells, and then further culture for 48 h at 21 °C. The bacterial cells were harvested through centrifugation, and the pellet was dissolved in PBS buffer (pH 6.5). Various level of salt treatment (0, 100 mM and 200 mM NaCl) and arsenic (sodium arsenate) treatment (10 µM) were given to produce H₂O₂ inside the bacterial cells. The 180 µL bacterial cells expressing nanosensor protein was transferred to 96-well plate and the FRET ratio was recorded for 420 s at regular interval of 60 s under normal conditions after the addition of 20 µL of different concentrations of H₂O₂ (0 mM, 0.5 mM and 1 mM). FRET ratio was also recorded under stress conditions (with arsenic and NaCl). Initially, fluorescence emission of acceptor and donor was measured for baseline correction and then measurement of the FRET ratio was done after 2 min of the addition of 10 µM arsenic (sodium arsenate) and 100 mM and 200 mM NaCl. The measurements were taken for further 18 min at every 2 min internals.

2.6. H_2O_2 Dynamics in Yeast under Normal and Stress Conditions

Live cell imaging of FLIP- H_2O_2 expressing yeast cells, and dynamics of H_2O_2 in the yeast cells under stress conditions using FLIP- H_2O_2 were carried out in the presence of arsenic and salt treatment (200 mM) for 10 min as per the protocol of Mohsin and Ahmad [19]. *Saccharomyces cerevesie* strain BY4742 was transformed with gateway cloned pYES-DEST-ECFP_RD_mVenus. The dual emission intensity ratio (mVenus(Y)/ECFP(C) ratio) was monitored by using confocal microscope (SP5, Leica Microsystems, Wetzlar, Germany) which is controlled by LAS-AF (Leica Application Suite-Advanced Fluorescence) software (Leica, Germany).

2.7. Monitoring of H_2O_2 Changes in Mammalian Cells

Live cell imaging and measurement of the change in the level of the H_2O_2 in the mammalian cells (HeLa cells) expressing FLIP- H_2O_2 was carried out as per Ahmad et al. [22].

3. Results and Discussion

3.1. Designing, Construction and Spectral Analysis of FLIP- H_2O_2

In this study, a genetically encoded nanosensor was developed for non-invasive real-time measurement of H_2O_2 in living cells by using bright fluorophores and advanced fluorescence imaging. The regulatory domain (RD) of OxyR, a member of the LysR family of bacterial transcription factor, was used as a ligand sensory domain (Supplementary Figure S1). Previous studies reported that the regulatory domain binds to H_2O_2 and an intramolecular disulphide bond is formed between Cys-199 and Cys-208 due to which structural changes occur in the regulatory domain that fetches both termini close to each other [23]. The RD of OxyR in reduced and oxidized form was shown in supplemental Figure S9. Significant conformational changes occurred in RD due to the disulphide bond formation between specific cysteines residues (Supplementary Figure S10). The two variants of green fluorescent protein were ligated with the H_2O_2 sensory domain, RD, at the N and C-terminus, respectively. For the development of these genetically encoded FRET sensors, the prerequisite is that the ligand sensory domain must be undergoing the appropriate conformational changes, which is translated the ligand binding into the FRET [24]. The sensing element, RD, fulfils this criterion of FRET as there was significant variation in the emission intensity of acceptor and donor fluorophore with the addition of the H_2O_2 . The schematic mechanism of FLIP- H_2O_2 sensor is represented in Figure 1A. Spectral analysis was done for the validation of expressed nanosensor protein. The nanosensor protein showed changes in the fluorescence emission intensities of ECFP and mVenus in the presence of H_2O_2 . Addition of H_2O_2 decreases the emission intensity of ECFP and increases the emission intensity of mVenus confirming that FRET is occurring in the presence of H_2O_2 with the nanosensor protein (Figure 1B).

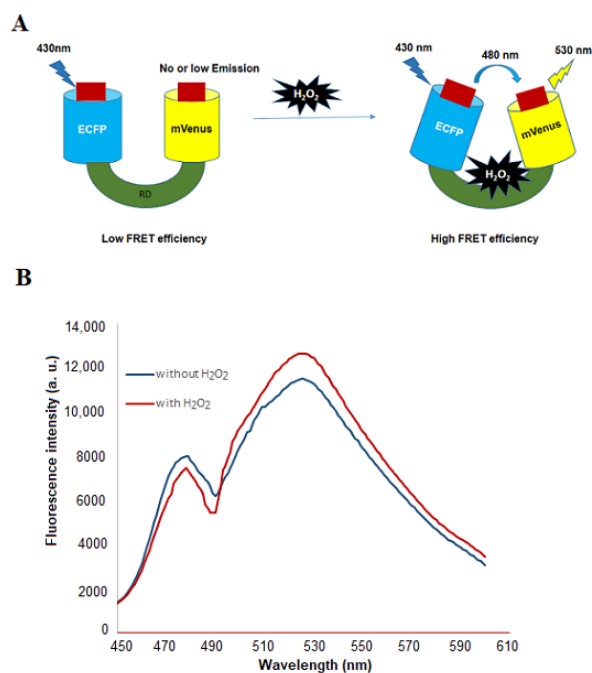


Figure 1. Schematic representation of the FLIP- H_2O_2 nanosensor. (A) Regulatory domain is attached with donor (ECFP) and acceptor (mVenus). Binding of H_2O_2 with the RD brings the donor and acceptor in close proximity and at this stage, emission of ECFP results in the transfer of energy and excites the mVenus. Ratio changes occur in the mVenus/ECFP emission by H_2O_2 . (B) Spectral analysis was performed using purified sensor protein.

3.2. *In Vitro* Characterization of FLIP- H_2O_2 Nanosensor

Fluorescent proteins are pH-sensitive, and their stability depends on the pH and composition of the buffer. To test the pH sensitivity and stability of nanosensor, fluorescence measurements were performed in different buffers (PBS, MOPS, Tris-Cl, and TBS) and at various pH ranges (5.0–8.0). The nanosensor protein exhibit the optimum stability in the PBS buffer (pH 7.0), as with this buffer the least changes in the FRET ratio were observed (Figure 2A). In the absence of H_2O_2 , the purified protein showed no change in FRET ratio. However, after the addition of H_2O_2 to the purified sensor protein, which is suspended in PBS buffer, the variation in FRET ratio was found (Figure 2A). Therefore, PBS buffer (pH 7.0) was selected to carry out further investigation of nanosensor. Specificity of the nanosensor was measured *in vitro* with various oxidants. The addition of oxidants such as super-oxide anion, nitric oxide and peroxynitrite did not cause any significant change in the FRET ratio of sensor protein (Figure 2B).

To find out the saturation limit and K_d of nanosensor protein, a titration experiment was conducted with nanosensor protein by adding the H_2O_2 from nanomolar to millimolar series (Figure 3). The calculated affinity (K_d) of sensor with the H_2O_2 was found to be 247 μM . FRET ratio measurement approach based on donor and acceptor fluorophore emission intensities has previously been used for the monitoring of antioxidants and amino acids [25,26]. In case of Hyper, authors showed sub-micromolar affinity for H_2O_2 in bacterial cells and higher affinity in HeLa cells and reported that in living cells at least 5 μM H_2O_2 is required to induce the fluorescence changes [15]. Exact K_d value was not mentioned in this case, however we expect this value to be around 8 μM . K_d reported in the literature for these systems is comparable with K_d value reported in our case and it is in this range. Limit of detection reported in case of the other H_2O_2 sensor was in the range of 1 to 200 μM [12,27,28]. FLIP- H_2O_2 showed a detection range from sub-micromolar to micromolar range (~ 0.1 to 563 μM). Sensor based on FRET offers higher dynamic range in terms of detection. For superior performance at nanomolar level, its limit of detection can further be improved in future. A comparative analysis of major H_2O_2 detection method has been presented in Supplementary Table S1.

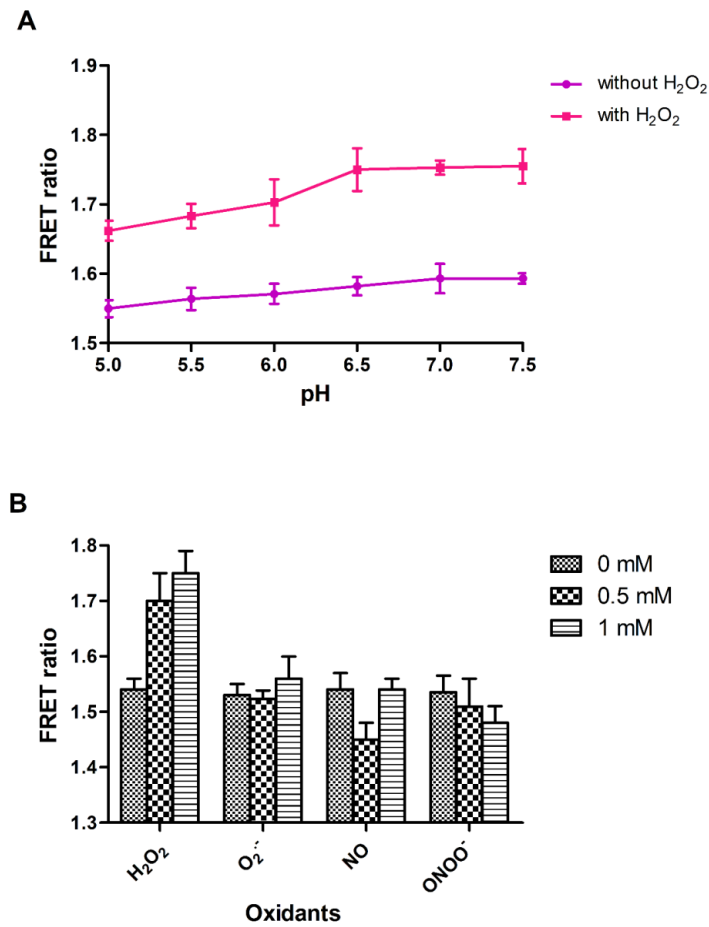


Figure 2. In vitro analysis of FLIP-H₂O₂. **(A)** pH stability analysis of FLIP-H₂O₂. **(B)** Specificity analysis of the FLIP-H₂O₂ nanosensor. (H₂O₂—hydrogen peroxide, O₂⁻—superoxide anions, NO—nitric oxide, ONOO⁻—peroxynitrite). Data are mean of three independent experiments. Vertical bars represent the standard error.

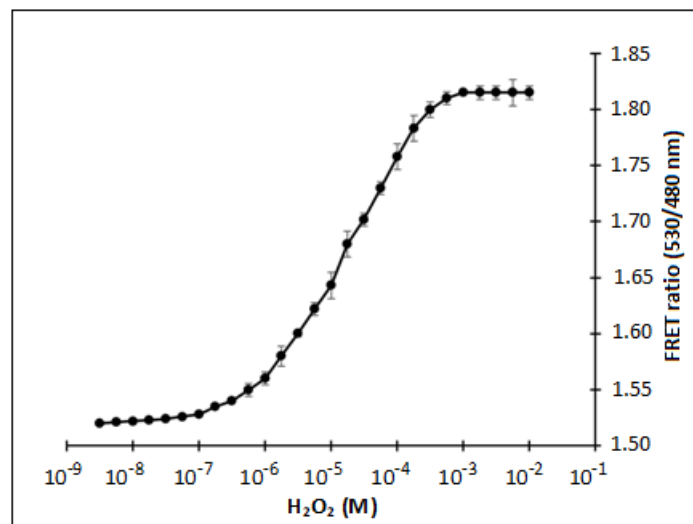


Figure 3. In vitro titration analysis of FLIP-H₂O₂ with various concentration of H₂O₂, the sigmoidal graph representing the changes in the Fluorescence Resonance Energy Transfer (FRET) ratio at very low to high concentration of H₂O₂ and saturation of FLIP-H₂O₂ nanosensor. Data are mean of three independent experiments. Vertical bars represent the standard error.

3.3. Intracellular H_2O_2 Flux Monitoring in Bacterial Cells

For *in vivo* H_2O_2 flux analysis, the *E. coli* BL21 cells were transformed with pGWF1-ECFP_RD_mVenus and allowed to express in the cytosol. The harvested bacterial cells were resuspended in PBS buffer and then resuspended bacterial cells were transferred to microplate wells and supplemented with H_2O_2 . After a fixed interval, the emission intensities of both fluorophores were recorded using fluorescence plate reader. An increase in the FRET ratio from 1.53 to 1.70 and 1.53 to 1.75 after the addition of 0.5 mM and 1 mM of H_2O_2 , respectively (Figure 4). Previously, the measurement of metabolite and ion accumulation was also performed inside the bacterial cells using FRET-based nanosensors [26,29].

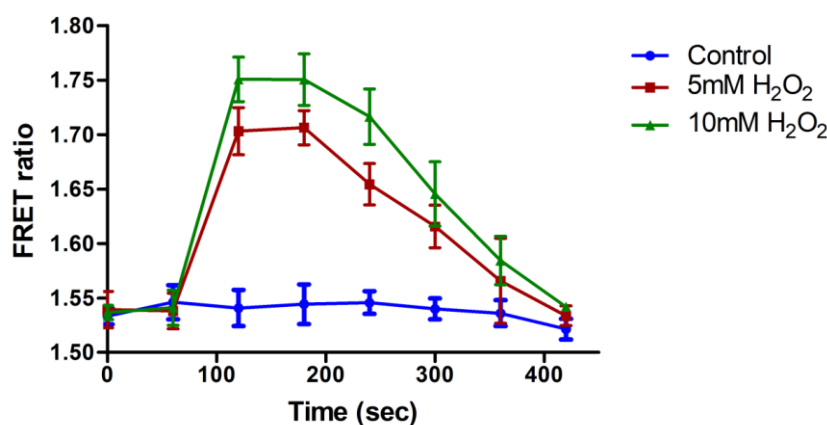


Figure 4. *In vivo* H_2O_2 flux analysis using FLIP- H_2O_2 . Nanosensor expressing bacterial cells were incubated with various concentration of H_2O_2 and FRET ratio was monitored for 420 s. Data are the mean of three independent experiments. Vertical bars represent the standard error.

3.4. Monitoring of H_2O_2 in Yeast and Mammalian Cells

Real-time confocal imaging data obtained from sensor transformed yeast cells indicated that the FLIP- H_2O_2 was expressed in the cytosol (Figure 5A) and allowed monitoring of H_2O_2 inside the cells. After one minute of addition of H_2O_2 , FLIP- H_2O_2 expressing yeast cells showed an increase in the FRET ratio from 1.42 to 1.55 (Figure 5B). Live cell imaging was also performed earlier for the monitoring of 2-oxoglutarate and ajmalacine in yeast cells using FRET-based 2-oxoglutarate and ajmalacine nanosensors [30,31].

In the case of yeast, nanosensor showed a kind of fluorescence quenching which was reflected in the form of initial low fluorescence intensity. Nanosensor had reacted to the H_2O_2 fast, so it reached to the saturation quickly after addition in these cells. Confocal imaging of transiently transfected HeLa cells with FLIP- H_2O_2 showed that FLIP- H_2O_2 distributed predominantly in the cytoplasm of cultured cells (Figure 6A). Non-invasive analysis of transfected HeLa cells showed an increase in the FRET ratio from 1.51 to 1.66 and 1.50 to 1.62 by the addition of H_2O_2 and NaCl respectively (Figure 6B). NaCl induced H_2O_2 production was also reported in endothelial cells where it was observed that the extracellular volume expands due to increased salt intake and induces the activation of transforming growth factor- β (TGF- β) [32]. However, TGF- β increases endothelial NADPH (nicotinamide adenine dinucleotide phosphate) oxidase-4 [33], an enzyme that induces the production of H_2O_2 [34].

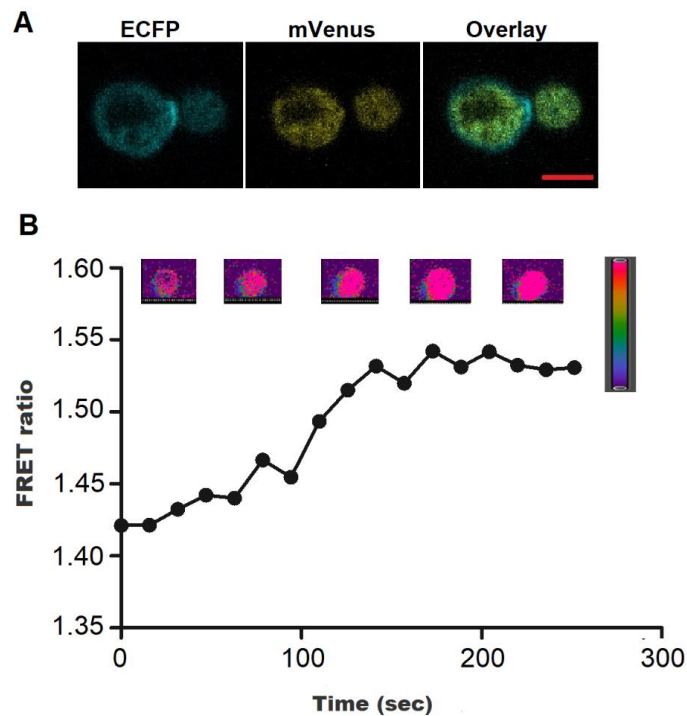


Figure 5. Flux monitoring of H_2O_2 in the cytosol of yeast cells. (A) Confocal images of yeast cells expressing the FLIP- H_2O_2 , showing ECFP, mVenus and Overlay (Scale bar = 2 μm). (B) H_2O_2 was added externally to the yeast cells after 1 min of laser scan and ratiometric images were recorded at defined intervals. Data are the mean of three independent experiments. Vertical bars represent the standard error.

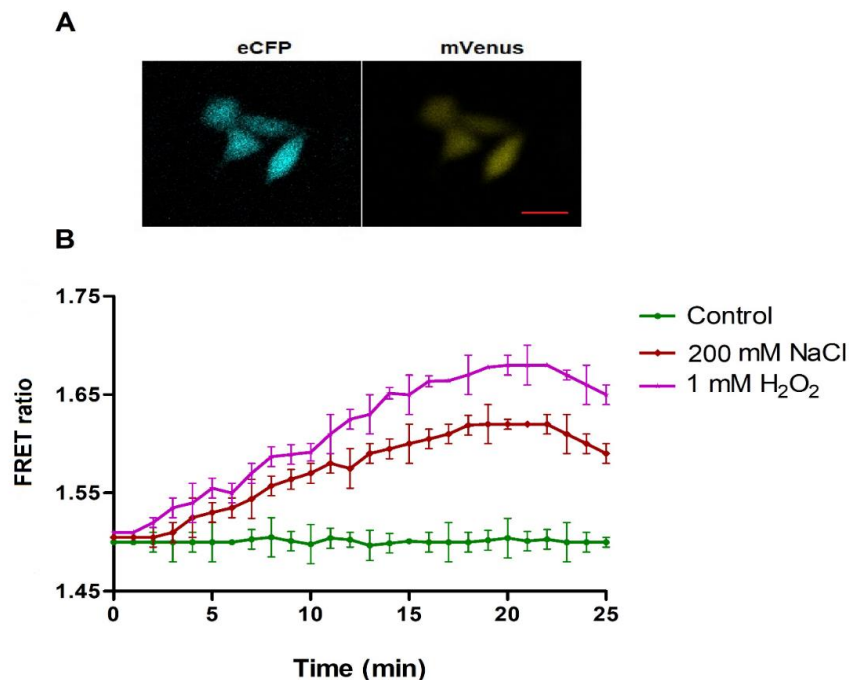


Figure 6. Flux monitoring of H_2O_2 in mammalian cells. (A) Confocal imaging of FLIP- H_2O_2 transformed mammalian cells (Scale bar = 10 μm). (B) Time dependent acceptor/donor intensity ratio change in single HeLa cells in the presence of externally supplied H_2O_2 and NaCl. Data are mean of three independent experiments. Vertical bars represent the standard error.

3.5. In Vivo H₂O₂ Flux Monitoring under Stress Conditions

To analyze and monitor the effect of abiotic stress conditions on the generation of H₂O₂, NaCl and arsenic were provided externally and fluorescence intensity changes were monitored in a ratiometric manner in FLIP-H₂O₂ expressing yeast and bacterial cells using microplate reader. For the generation of abiotic stress, we treated bacterial and yeast cells with different concentrations of NaCl and arsenic, separately. FRET ratio was monitored at the interval of 2 min for 18 min. In the first 2 min, no significant change in the FRET ratio was observed because the expression of stress producing enzymes and synthesis of H₂O₂ in bacterial and yeast cells takes time. In arsenic and salt treated cells, an increase in the FRET ratio was observed after 2 min, which was increased up to 10 min and then become saturated (Figures 7 and 8A,B). At the saturation point, ascorbate was added to check and measure the effect of this antioxidant on cellular H₂O₂. Nanosensor reports the decreased level of H₂O₂ inside the bacterial cells in the presence of ascorbate (Figure 7), which indicate its antioxidant property. Experimental results have indicated the generation of H₂O₂ after exposure to arsenic in Chinese hamster ovary cells [35].

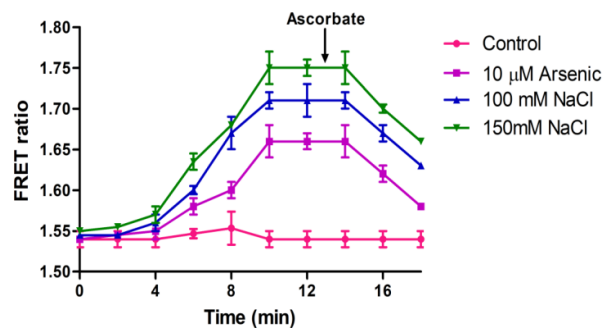


Figure 7. Change in the FRET ratio in the presence of different concentration of salt and arsenic in the bacterial cells expressing FLIP-H₂O₂. Data are mean of three independent experiments. Vertical bars represent the standard error.

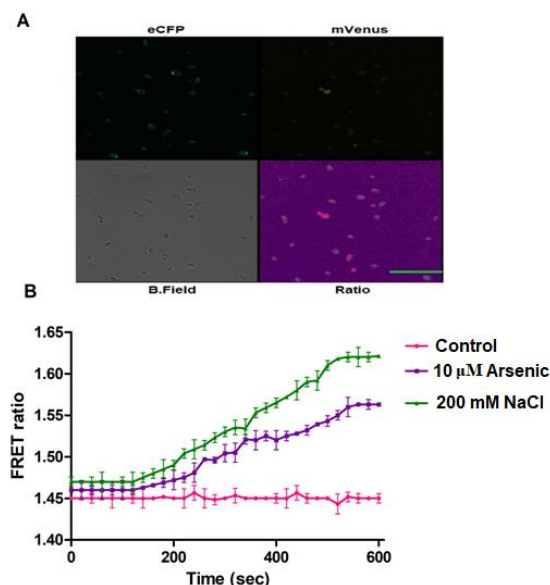


Figure 8. (A) Confocal microscopy imaging of nanosensor expressing yeast cells showing ECFP, mVenus, bright field and ratio images at various channels (Scale bar = 20 μm.). (B) Ratiometric measurements of H₂O₂ was performed in yeast cells after one minute of addition of As³⁺ and NaCl. Data are the mean of three independent experiments. Vertical bars represent the standard error.

4. Conclusions

Understanding how living cells cope with environmental change requires a Spatio-temporal perspective. The development and adaptation of a FRET nanosensor provides the capacity to visualize changes in the transport and accumulation of metabolites and small molecules at the cellular level, which is required to identify the regulatory switches in the metabolic network. Flux monitoring of H₂O₂ in the cytosol of living bacterial, yeast and mammalian cells demonstrate that the FLIP-H₂O₂ is an excellent tool for non-invasive real-time monitoring of H₂O₂ in any cell type. Moreover, attachment of sub-cellular targeting signal to the FLIP-H₂O₂ will facilitate in vivo monitoring of H₂O₂ in key cellular organelles, such as chloroplasts, mitochondria. Therefore, live imaging approaches coupled with automated image-analysis algorithms are revealing new levels of dynamism and plasticity of the cellular response. Together, these tools will offer a more comprehensive understanding of environmental responses in cellular organisms.

Supplementary Materials: The following are available online at <http://www.mdpi.com/2079-7737/9/12/0430/s1>, Figure S1: Crystal structure of regulatory domain of OxyR which was used as sensory element, Figure S2, Schematic representation of pDONR-RD, Figure S3, Representation of full construct of pGWF1-ECFP-RD-mVenus, Figure S4, Restriction digestion of pGWF1-ECFP-RD-mVenus plasmid. Digested product was resolved on 1% agarose gel and visualized by EtBr/UV, Figure S5, Nucleotides sequences of the FLIP-H₂O₂ sensor, Figure S6, Schematic representation of pYES-DEST-ECFP-RD-mVenus, Figure S7, Schematic representation of pcDNA-ECFP-RD-mVenus, Figure S8, Purified ECFP-RD-mVenus protein was resolved on 12% SDS-PAGE. Expected band was observed (M-marker, S-purified protein ~80 kD), Figure S9, Reduced and oxidized form of RD and H₂O₂ induced conformational changes in the domain, Figure S10, Close-up structure of critical cysteine residues of Regulatory Domain involved in H₂O₂ sensing, Table S1, Comparison of various H₂O₂ detection approaches and their properties.

Author Contributions: Conceptualization, A., H.M.A., M.A., A.A.; formal analysis, A., M.A.; investigation, A., A.A.; methodology, A., H.M.A., M.A., A.A.; resources, H.M.A., A.A.; supervision, A.A., M.A.; validation, M.A., H.M.A.; writing—original draft, revision, A., H.M.A., M.A., A.A.; M.Z.M.S., writing—review and editing, revision. All authors have read and agreed to the published version of the manuscript.

Funding: This research received no external funding.

Acknowledgments: The authors gratefully acknowledge the Researchers Supporting Project number (RSP-2020/123) King Saud University, Riyadh, Saudi Arabia.

Conflicts of Interest: The authors declare no conflict of interest.

References

1. D’Aur eaux, B.; Toledano, M.B. ROS as signalling molecules: Mechanisms that generate specificity in ROS homeostasis. *Nat. Rev. Mol. Cell Biol.* **2007**, *8*, 813–824. [[CrossRef](#)]
2. Halliwell, B. Free radicals and antioxidants—quo vadis? *Trends Pharm. Sci.* **2011**, *32*, 125–130. [[CrossRef](#)] [[PubMed](#)]
3. Zentgraf, U. Oxidative stress and leaf senescence. *Annu. Plant Rev. Senescence Process. Plants* **2007**, *26*, 69–86.
4. Schieber, M.; Chandel, N.S. ROS function in redox signaling and oxidative stress. *Curr. Biol.* **2014**, *24*, 453–462. [[CrossRef](#)] [[PubMed](#)]
5. Smirnov, N.; Arnaud, D. Hydrogen peroxide metabolism and functions in plants. *New Phytol.* **2019**, *221*, 1197–1214. [[CrossRef](#)]
6. Costa, A.; Drago, I.; Behera, S.; Zottini, M.; Pizzo, P.; Schroeder, J.I.; Pozzan, T.; Schiavo, F.L. H₂O₂ in plant peroxisomes: An in vivo analysis uncovers a Ca²⁺-dependent scavenging system. *Plant J.* **2010**, *62*, 760–772. [[CrossRef](#)]
7. Doke, N. Generation of superoxide anion by potato tuber protoplasts during the hypersensitive response to hyphal wall components of *Phytophthora infestans* and specific inhibition of the reaction by suppressors of hypersensitivity. *Physiol. Plant Pathol.* **1983**, *23*, 359–367. [[CrossRef](#)]
8. Thordal-Christensen, H.; Zhang, Z.; Wei, Y.; Collinge, D.B. Subcellular localization of H₂O₂ in plants. H₂O₂ accumulation in papillae and hypersensitive response during the barley—Powdery mildew interaction. *Plant J.* **1997**, *11*, 1187–1194. [[CrossRef](#)]

9. Dikalov, S.I.; Harrison, D.G. Methods for detection of mitochondrial and cellular reactive oxygen species. *Antioxid. Redox Signal.* **2014**, *20*, 372–382. [[CrossRef](#)]
10. Miller, E.W.; Albers, A.E.; Pralle, A.; Isacoff, E.Y.; Chang, C.J. Boronate-based fluorescent probes for imaging cellular hydrogen peroxide. *J. Am. Chem. Soc.* **2005**, *127*, 16652–16659. [[CrossRef](#)]
11. Dickinson, B.C.; Huynh, C.; Chang, C.J. A palette of fluorescent probes with varying emission colors for imaging hydrogen peroxide signaling in living cells. *J. Am. Chem. Soc.* **2010**, *132*, 5906–5915. [[CrossRef](#)] [[PubMed](#)]
12. Albers, A.E.; Okreglak, V.S.; Chang, C.J. A FRET-based approach to ratiometric fluorescence detection of hydrogen peroxide. *J. Am. Chem. Soc.* **2006**, *128*, 9640–9641. [[CrossRef](#)] [[PubMed](#)]
13. Nietzel, T.; Elsässer, M.; Ruberti, C.; Steinbeck, J.; Ugalde, J.M.; Fuchs, P.; Wagner, S.; Ostermann, L.; Moseler, A.; Lemke, P.; et al. The fluorescent protein sensor ro GFP 2-Orp1 monitors in vivo H₂O₂ and thiol redox integration and elucidates intracellular H₂O₂ dynamics during elicitor-induced oxidative burst in Arabidopsis. *New Phytol.* **2019**, *221*, 1649–1664. [[CrossRef](#)] [[PubMed](#)]
14. Hanson, G.T.; Aggeler, R.; Oglesbee, D.; Cannon, M.; Capaldi, R.A.; Tsien, R.Y.; Remington, S.J. Investigating mitochondrial redox potential with redox-sensitive green fluorescent protein indicators. *J. Biol. Chem.* **2004**, *279*, 13044–13053. [[CrossRef](#)]
15. Belousov, V.V.; Fradkov, A.F.; Lukyanov, K.A.; Staroverov, D.B.; Shakhbazov, K.S.; Terskikh, A.V.; Lukyanov, S. Genetically encoded fluorescent indicator for intracellular hydrogen peroxide. *Nat. Methods* **2006**, *3*, 281–286. [[CrossRef](#)]
16. Okumoto, S.; Jones, A.; Frommer, W.B. Quantitative imaging with fluorescent biosensors. *Annu. Rev. Plant Biol.* **2012**, *63*, 663–706. [[CrossRef](#)]
17. Hochreiter, B.; Pardo-Garcia, A.; Schmid, J.A. Fluorescent proteins as genetically encoded FRET biosensors in life sciences. *Sensors* **2015**, *15*, 26281–26314. [[CrossRef](#)]
18. Vinkenborg, J.L.; Nicolson, T.J.; Bellomo, E.A.; Koay, M.S.; Rutter, G.A.; Merckx, M. Genetically encoded FRET sensors to monitor intracellular Zn²⁺ homeostasis. *Nat. Methods* **2009**, *6*, 737. [[CrossRef](#)]
19. Mohsin, M.; Ahmad, A. Genetically-encoded nanosensor for quantitative monitoring of methionine in bacterial and yeast cells. *Biosens. Bioelectron.* **2014**, *59*, 358–364. [[CrossRef](#)]
20. Ballerstadt, R.; Gowda, A.; McNichols, R. Fluorescence resonance energy transfer-based near-infrared fluorescence sensor for glucose monitoring. *Diabetes Technol. Ther.* **2004**, *6*, 191–200. [[CrossRef](#)]
21. Waadt, R.; Hitomi, K.; Nishimura, N.; Hitomi, C.; Adams, S.R.; Getzoff, E.D.; Schroeder, J.I. FRET-based reporters for the direct visualization of abscisic acid concentration changes and distribution in Arabidopsis. *Elife* **2014**, *3*, e01739. [[CrossRef](#)] [[PubMed](#)]
22. Ahmad, M.; Mohsin, M.; Iqar, S.; Manzoor, O.; Siddiqi, T.O.; Ahmad, A. Live cell imaging of vitamin B12 dynamics by genetically encoded fluorescent nanosensor. *Sens. Actuator B Chem.* **2018**, *257*, 866–874. [[CrossRef](#)]
23. Zheng, M.; Åslund, F.; Storz, G. Activation of the OxyR transcription factor by reversible disulfide bond formation. *Science* **1998**, *279*, 1718–1722. [[CrossRef](#)] [[PubMed](#)]
24. Fehr, M.; Frommer, W.B.; Lalonde, S. Visualization of maltose uptake in living yeast cells by fluorescent nanosensors. *Proc. Natl. Acad. Sci. USA* **2002**, *99*, 9846–9851. [[CrossRef](#)] [[PubMed](#)]
25. Ahmad, M.; Anjum, N.A.; Asif, A.; Ahmad, A. Real-time monitoring of glutathione in living cells using genetically encoded FRET-based ratiometric nanosensor. *Sci. Rep.* **2020**, *10*, 1–9. [[CrossRef](#)]
26. Ahmad, M.; Ameen, S.; Siddiqi, T.O.; Khan, P.; Ahmad, A. Live cell monitoring of glycine betaine by FRET-based genetically encoded nanosensor. *Biosens. Bioelectron.* **2016**, *86*, 169–175. [[CrossRef](#)]
27. Yu, D.; Wang, P.; Zhao, Y.; Fan, A. Iodophenol blue-enhanced luminol chemiluminescence and its application to hydrogen peroxide and glucose detection. *Talanta* **2016**, *146*, 655–661. [[CrossRef](#)]
28. Gutscher, M.; Sobotta, M.C.; Wabnitz, G.H.; Ballikaya, S.; Meyer, A.J.; Samstag, Y.; Dick, T.P. Proximity-based protein thiol oxidation by H₂O₂-scavenging peroxidases. *J. Biol. Chem.* **2009**, *284*, 31532–31540. [[CrossRef](#)]
29. Bischof, H.; Rehberg, M.; Stryeck, S.; Artinger, K.; Eroglu, E.; Waldeck-Weiermair, M.; Gottschalk, B.; Rost, R.; Deak, A.T.; Niedrist, T.; et al. Novel genetically encoded fluorescent probes enable real-time detection of potassium in vitro and in vivo. *Nat. Commun.* **2017**, *8*, 1–12. [[CrossRef](#)]
30. Zhang, C.; Ye, B.C. A single fluorescent protein-based sensor for in vivo 2-oxoglutarate detection in cell. *Biosens. Bioelectron.* **2014**, *54*, 15–19. [[CrossRef](#)]

31. Ambrin, G.; Ahmad, M.; Alqarawi, A.A.; Hashem, A.; Abd_Allah, E.F.; Ahmad, A. Conversion of cytochrome P450 2D6 of human into a FRET-based tool for real-time monitoring of Ajmalicine in living cells. *Front. Bioeng. Biotechnol.* **2019**, *7*, 375. [[CrossRef](#)] [[PubMed](#)]
32. Ying, W.Z.; Aaron, K.; Sanders, P.W. Mechanism of dietary salt-mediated increase in intravascular production of TGF- β 1. *Am. J. Physiol. Renal Physiol.* **2008**, *295*, 406–414. [[CrossRef](#)] [[PubMed](#)]
33. Thannickal, V.J.; Hassoun, P.M.; White, A.C.; Fanburg, B.L. Enhanced rate of H₂O₂ release from bovine pulmonary artery endothelial cells induced by TGF-beta 1. *Am. J. Physiol. Lung Cell Mol. Physiol.* **1993**, *265*, 622–626. [[CrossRef](#)] [[PubMed](#)]
34. Nisimoto, Y.; Diebold, B.A.; Cosentino-Gomes, D.; Lambeth, J.D. Nox4: A hydrogen peroxide-generating oxygen sensor. *Biochemistry* **2014**, *53*, 5111–5120. [[CrossRef](#)]
35. Wang, T.S.; Kuo, C.F.; Jan, K.Y.; Huang, H. Arsenite induces apoptosis in chinese hamster ovary cells by generation of reactive oxygen species. *J. Cell. Physiol.* **1996**, *169*, 256–268. [[CrossRef](#)]

Publisher’s Note: MDPI stays neutral with regard to jurisdictional claims in published maps and institutional affiliations.



© 2020 by the authors. Licensee MDPI, Basel, Switzerland. This article is an open access article distributed under the terms and conditions of the Creative Commons Attribution (CC BY) license (<http://creativecommons.org/licenses/by/4.0/>).